Entropy Generation for MHD Radiative Variable Thermal Conductivity Nanofluid Flow through Porous Channel

Md. S. Alam*
Department of Mathematics, Jagannath University,
Dhaka-1100, Bangladesh

M. A. H. Khan
Department of Mathematics, Bangladesh University of Engineering and Technology,
Dhaka-1000, Bangladesh

M. A. Alim
Department of Mathematics, Bangladesh University of Engineering and Technology,
Dhaka-1000, Bangladesh

Abstract

The radiative heat transfer performance with viscous dissipation on entropy generation in the MHD flow of variable thermal conductivity viscous Cu–water nanofluid through a porous parallel channel is investigated in this paper. The governing non-linear differential equations are solved using power series for small values of thermal conductivity variation parameter, which are then analysed by Hermite- Padé approximation method. The effects of the physical governing flow parameters on velocity, temperature and entropy generation are discussed extensively both numerically and graphically. A stability analysis has been performed for the local rate of heat transfer which signifies that the lower solution branch is stable and physically acceptable. The entropy generation of the system increases at the two porous plates and also the fluid friction irreversibility is dominant there.

Keywords: Porous Channel; Thermal radiation; variable thermal conductivity; Nanofluid; Entropy generation; bifurcation.

1. Introduction

The flow and heat transfer in porous tubes or channels has been studied by a number of authors ([1], [2], [3]) because of its various applications in biomedical engineering, material processing, as well as the food and petro-chemical industries. Berman [4] described an exact solution of the Navier-Stokes equation for steady two-dimensional laminar flow of a viscous, incompressible fluid in a channel with parallel rigid porous walls driven by uniform suction or injection at the walls. Meanwhile, heat transfer acts a significant role in many fields where the heating and cooling processes involved. Any substance with a temperature above absolute zero transfers heat in the form of radiation. Thermal radiation always exits and can strongly interact with convection in many situations of engineering interest. However, radiative heat transfer has a key impact in high temperature regime. Many technological processes occur at high temperature and good working knowledge of radiative heat transfer plays an instrumental

role in designing the relevant equipment. In Cogley *et al.* [5], the differential approximation for radiative heat transfer in a nonlinear equation for gray gas near equilibrium was proposed. Chawla and Chan [6] studied the effect of radiative heat transfer on thermally developing Poiseuille flow with scattering. The thermal conductivity of the fluid had been assumed to be constant in all the above studies. However, it is known that this physical property may be change significantly with temperature. For a liquid, it has been found that the thermal conductivity κ varies with temperature in an approximately linear manner in the range from 0 to 400^0F, as Kay [7]. Pinarbasi *et al.* [8] investigates the effect of variable viscosity and thermal conductivity of a non-isothermal, incompressible Newtonian fluid flowing under the effect of a constant pressure gradient at constant temperatures in plane Poiseuille flow using Chebyshev pseudospectral method.

In the past few years, several simple flow problems associated with classical hydrodynamics have received new attention within the more general context of magnetohydrodynamics (MHD). A survey of MHD studies in the technological fields can be found in Moreau [9]. Makinde [10] analysed magnetohydrodynamic stability of Plane Poiseuille flow using multideck asymptotic technique. It is observed in his analysis that the magnetic field has a stabilizing effect on the flow and that this stability increases with an increase in Hartmann number. Patra et al. [11] examined radiation effect on MHD fully developed mixed convection in a vertical channel with asymmetric heating where they observed that an increase in radiation parameter leads to a decrease in the fluid temperature in the channel.

Heat transfer efficiency can be improved by increasing the thermal conductivity of the working fluid as Kwak and Kim [12]. Due to heat transfer mostly used fluids such as water, ethylene glycol, and engine oil have relatively low thermal conductivities compared to the thermal conductivity of solids. High thermal conductivity of solids can be used to increase the thermal conductivity of a fluid by adding small solid particles to that fluid. The feasibility of the usage of such suspensions of solid particles with sizes on the order of millimeters or micrometers was investigated by various researchers and significant advantages were observed in Khanafer et al. [13]. Recent advances in nanotechnology have allowed authors to study the next generation nanofluids, a term first introduced by Choi [14]. Nanoparticles have unique chemical and physical properties and have better thermal conductivity and radiative heat transfer compared to the base fluid only. Nanofluids are engineered dilute colloidal dispersions of nano-sized (less than 100 nm) particles in a base-fluid [15]. Sheikholeslami et al. [16] investigated analytically the laminar nanofluid flow in a semi-porous channel in the presence of transverse magnetic field using Homotopy perturbation method.

For any thermal system, as the entropy generation increases, the energy decreases. Thus, to enhance the efficiency of the system, the rate of entropy generation must be effectively controlled. The idea of thermodynamic irreversibility is central to the understanding of entropy. Everyone has an intuitive knowledge of irreversibility. The second law of thermodynamics states that all real processes are irreversible. Entropy generation provides a measure of the amount of irreversibility associated with real process. Bejan [17] studied the entropy-generation for forced convective heat transfer due to temperature gradient and viscosity effects in a fluid. Bejan [18] also presented various reasons for entropy-generation in applied thermal engineering where the generation of entropy destroys the available work of a system. The effect of thermal radiation and variable viscosity on entropy generation rate

in the flow of optically thin fluid through channel was analysed by Makinde [19]. However, the thermal boundary layer equation for variable thermal conductivity fluids in the presence of thermal radiation construct a nonlinear problem and the solution behavior will present a looming into physical process of thermal instability in the system. Chen et al. [20] studied heat transfer and entropy generation in fully-developed mixed convection nanofluid flow in vertical channel. They analysed the effects of viscous dissipation on the entropy generation within vertical asymmetrically heated channels containing mixed convection flow. Abiodun et al. [21] investigated entropy generation in a steady flow of viscous incompressible fluids between two infinite parallel porous plates for two different physical situations Couette flow and pressure-driven Poiseuille flow. Makinde and Eegunjobi [22] analysed the combined effects of convective heating and suction/injection on entropy generation rate in a channel with permeable walls.

Taking into account the significance of variable thermal conductivity and thermal radiation effect on entropy generation rate in the flow of MHD conducting viscous nanofluid through a porous channel with non-uniform wall temperature is studied applying Hermite- Padé approximation. A stability analysis is also performed to show the physically realizable solution in practice of local Nusselt number due to thermal conductivity criticality. Results for the velocity, temperature, volumetric entropy generation rate and Bejan number for various values of the involved parameters are presented.

2. Mathematical Formulation

The two-dimensional steady, incompressible and laminar variable thermal conductivity flow of Cu-water nanofluid in a porous channel is considered. The lower and upper walls of the channel are assumed to be porous as injection and suction respectively

so that $\vec{V} = (u', v', 0)$ where u' and v' are the horizontal and vertical (injection/suction) components of velocity respectively. The flow is chosen along the x'-direction under constant pressure gradient and depends on y' alone. The top and bottom wall temperatures are non-uniform under radiative heat transfer and an externally homogeneous magnetic field is applied vertically to the upper wall. The basic equations of the problem considering viscous dissipation and buoyancy force are

$$\frac{\partial u'}{\partial x'} + \frac{\partial v'}{\partial y'} = 0 \tag{1}$$

$$u'\frac{\partial u'}{\partial x'} + v'\frac{\partial u'}{\partial y'} = -\frac{1}{\rho_{nf}}\frac{\partial p'}{\partial x'} + \nu_{nf}\left(\frac{\partial^2 u'}{\partial x'^2} + \frac{\partial^2 u'}{\partial y'^2}\right)$$
$$-\frac{\sigma_{nf}B_0^{\,2}}{\rho_{nf}}u' + g\beta(\bar{T} - T_0) \tag{2}$$

$$(\rho c_p)_{nf}\left(u'\frac{\partial \bar{T}}{\partial x'} + v'\frac{\partial \bar{T}}{\partial y'}\right) = \kappa_{nf}\left(\frac{\partial^2 \bar{T}}{\partial x'^2} + \frac{\partial^2 \bar{T}}{\partial y'^2}\right)$$
$$+ \mu_{nf}\left(\frac{\partial u'}{\partial y'}\right)^2 - \frac{\partial q}{\partial y'} \tag{3}$$

As the velocity is only along x'-direction, it is assumed that

$$\frac{\partial u'}{\partial x'} = 0, \ \frac{\partial \bar{T}}{\partial x'} = 0, \ \frac{\partial^2 \bar{T}}{\partial x'^2} = 0.$$

By integrating Eqn (1) reduces to $v' = v_0$. Equations (2) and (3) then take the form

$$\frac{d^2 u'}{dy'^2} - \frac{v_0}{\nu_{nf}}\frac{du'}{dy'} - \frac{1}{\mu_{nf}}\frac{dp'}{dx'} - \frac{\sigma_{nf}B_0^{\,2}}{\mu_{nf}}u'$$
$$+ \frac{g\beta(\bar{T} - T_0)}{\nu_{nf}} = 0 \tag{4}$$

$$\frac{1}{(\rho c_p)_{nf}}\left[\begin{array}{c}\kappa_{nf}\dfrac{d^2 \bar{T}}{dy'^2} - (\rho c_p)_{nf}v_0\dfrac{d\bar{T}}{dy'} - \dfrac{dq}{dy'} \\[2mm] + \mu_{nf}\left(\dfrac{du'}{dy'}\right)^2\end{array}\right] = 0 \tag{5}$$

Where, the variable thermal conductivity $\kappa_{nf} = \kappa_\infty \left[1 + \alpha \dfrac{\bar{T} - T_a}{T_a - T_0}\right]$,

according to Kay [7], and k_∞ is the thermal conductivity at the ambient temperature T_0,

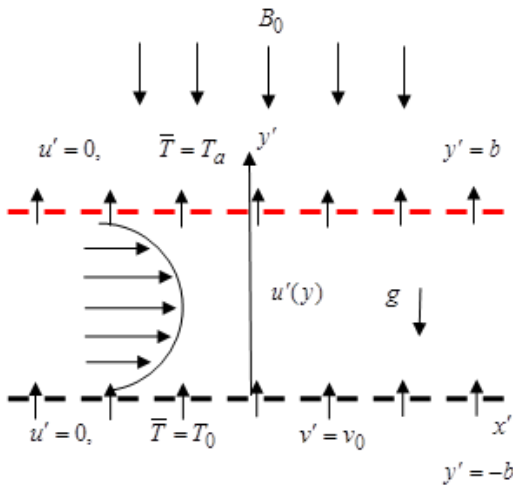α is defined by $\alpha = \dfrac{1}{\kappa_{nf}} \left(\dfrac{\partial \kappa}{\partial \bar{T}}\right)_{nf}$.

Fig.1. Geometry of the problem.

Eqs. (4)-(5) are subjected to the boundary conditions are:

$$y' = -b : \ u' = 0, \ \bar{T} = T_0$$
$$y' = b : \ u' = 0, \ \bar{T} = T_a \quad\quad (6)$$

The dynamic viscosity and density of the nanofluid are defined as Sheikholeslami et al. [16]

$$\mu_{nf} = \frac{\mu_f}{(1-\phi)^{2.5}}, \quad \rho_{nf} = (1-\phi)\rho_f + \phi\rho_s,$$

where ϕ is the solid volume fraction of nanoparticles.

The effective electrical conductivity, thermal conductivity and effective heat capacity of the nanofluid were presented by Sheikholeslami et al. [23] as:

$$\frac{\sigma_{nf}}{\sigma_f} = 1 + \left[3\left(\frac{\sigma_s}{\sigma_f} - 1\right)\phi \bigg/ \left(\left(\frac{\sigma_s}{\sigma_f} + 2\right) - \left(\frac{\sigma_s}{\sigma_f} - 1\right)\phi\right)\right]$$

$$k_{nf} = k_f \frac{k_s + 2k_f - 2\phi(k_f - k_s)}{k_s + 2k_f + \phi(k_f - k_s)}$$
$$(\rho c_p)_{nf} = (1-\phi)(\rho c_p)_f + \phi(\rho c_p)_s$$

The radiative heat flux according to Cogley et al. [5] is given by

$$\frac{dq}{dy'} = 4\gamma^2(\bar{T} - T_a)$$

$$\gamma^2 = \int_0^{y'} K_{\lambda a}\left(\frac{\partial e_{b\lambda}}{\partial \bar{T}}\right)_a d\lambda$$

where $K_{\lambda a}$ is the radiation absorption coefficient, λ is the wave length and $e_{b\lambda}$ is the Planks' function.

Introduce the following transformations to seek for a similarity solution of Eqs. (4)-(5)

$$x = \frac{x'}{b}, \ y = \frac{y'}{b}, \ u = \frac{u'}{v_0}, \ p = \frac{b\ p'}{\mu_f v_0}, \ \theta = \frac{\bar{T} - T_0}{T_a - T_0},$$

$$Ha'^2 = \frac{\sigma_f B_0^2 b^2}{\mu_f}, \ Gr' = \frac{g\beta(T_a - T_0)b^2}{\nu_f v_0}, \quad (7)$$

$$R' = \frac{4\gamma^2 b^2}{\kappa_\infty}, \ Br' = \frac{\mu_f v_0^2}{\kappa_\infty(T_a - T_0)}, \ N = -\frac{dp}{dx}, \ Re' = \frac{v_0 b}{\nu_f},$$

$$Pe' = \frac{v_0 b(\rho c_p)_f}{\kappa_\infty}, \ \kappa = \frac{\kappa_{nf}}{\kappa_\infty}, \ \kappa = 1 + \alpha\theta \quad (8)$$

Equations (4)-(5) in non-dimensional form are

$$\frac{d^2 u}{dy^2} - BCRe'\frac{du}{dy} - C(A\ Ha'^2 u - BGr'\theta - N) = 0$$

$$(9)\ [1 + \alpha\theta]\frac{d^2\theta}{dy^2} - BPe'\frac{d\theta}{dy} - R'\theta + \frac{Br'}{C}\left(\frac{du}{dy}\right)^2 = 0$$

$$(10)$$

Where,

$$A = 1 + \left[3\left(\frac{\sigma_s}{\sigma_f} - 1\right)\phi \bigg/ \left(\left(\frac{\sigma_s}{\sigma_f} + 2\right) - \left(\frac{\sigma_s}{\sigma_f} - 1\right)\phi\right)\right],$$

$$B = 1 - \phi + \phi\frac{\rho_s}{\rho_f} \text{ and } C = (1-\phi)^{2.5}$$

The boundary conditions in Eqn (6) reduce to following dimensionless form

$$y = -1 : \ u = 0, \ \theta = 0$$
$$y = 1 \ \ : \ u = 0, \ \theta = 1 \quad\quad (11)$$

Because of simplicity in calculation, the dimensionless numbers in Eqs (9)-(10) are rescaled as

$$Gr = \frac{Gr'}{\alpha}, \quad Ha^2 = \frac{Ha'^2}{\alpha}, \quad R = \frac{R'}{\alpha},$$
$$Br = \frac{Br'}{\alpha}, \quad \mathrm{Re} = \frac{\mathrm{Re}'}{\alpha}, \quad Pe = \frac{Pe'}{\alpha} \quad (12)$$

The dimensionless Eqs (9)-(10) get the form

$$\frac{d^2u}{dy^2} - BC\mathrm{Re}\alpha\frac{du}{dy} - C(AHa^2\alpha u - BGr\alpha\theta - N) = 0 \quad (13)$$

$$\frac{d^2\theta}{dy^2} + \alpha\theta\frac{d^2\theta}{dy^2} - BP\alpha\frac{d\theta}{dy} - R\alpha\theta + \frac{Br}{C}\alpha\left(\frac{du}{dy}\right)^2 = 0 \quad (14)$$

The local Nusselt number *Nu* and heat transfer rate are

$$Nu = \frac{q_w\big|_{y'=b}}{\kappa_f \Delta\bar{T}}, \quad q_w = -\kappa_{nf}\left(\frac{\partial\bar{T}}{\partial y'}\right) \quad (15)$$

From equations (8) and (15), the Nusselt number results in the following form

$$Nu = -\frac{\kappa_{nf}}{\kappa_f}\theta'(1) \quad (16)$$

3. Series analysis

The power series expansions are considered in terms of the parameter α as equations (13) and (14) are non-linear for velocity field and temperature distribution

$$u = \sum_{i=0}^{\infty} u_i\alpha^i, \quad \theta = \sum_{i=0}^{\infty} \theta_i\alpha^i, \quad |\alpha| < 1 \quad (17)$$

The non-dimensional governing equations (13) and (14) are then solved into series solutions by substituting the Eq. (17) and equating the coefficients of powers of α. The first 12 coefficients for the series of the temperature $\theta(\alpha)$ and velocity $u(\alpha)$ in terms of $\alpha, Ha, R, Gr, Br, N, \mathrm{Re}, Pe, A, B, C$ are computed. The first few coefficients of series for $\theta(\alpha)$ is given below:

$$\theta(y; \alpha, R, \mathrm{Re}, Pe, N, Gr, Br, Ha, A, B, C) = \frac{1}{2} + \frac{1}{2}y - \frac{1}{12}(y-1)$$
$$(y+1)(BrCN^2y^2 - Ry - 2BPe - 3R + BrCN^2)\alpha - \frac{1}{720}$$
$$(y-1)(y+1)(105R - 30BrCN^2 + 30yBPe + 90BPeR$$
$$-60B^2Pe^2y + 75R^2 + 60Ry + 90bPe + 15Ry^2 - 3R^2y^3$$
$$-15R^2y^2 + 7R^2y - 18BrCN^2y - 18BrCN^2y^3 - 30BPeRy^2$$
$$-60BPeRy - 28BrCN^2R - 30BrCN^2y^2 + 12BPeBrCN^2y$$
$$+2RBrCN^2y^2 + 12BPeBrCN^2y^3 + 2RBrCN^2y^4$$
$$+8ABrC^2N^2Ha^2y^4 + 36BrC^2N^2B\mathrm{Re}\,y^3$$
$$-52ABrC^2N^2Ha^2y^2 + 18BrCNGrBy^3 + 60BrCNGrBy$$
$$-2BrCNGrBy - 4BrC^2N^2B\mathrm{Re}\,y - 52BrC^2N^2AHa^2$$
$$+60BrCNBGr)\alpha^2 + O(\alpha^3) \quad ....(18)$$

The above power series solutions are valid for very small values of α. Therefore, the series are analysed applying Hermite- Padé approximation method, as demonstrated in the following section.

4. Hermite-Padé approximants.

The idea of thermal conductivity criticality or non-existence of steady-state solution to nonlinear thermal boundary layer equations for certain parameter values is extremely important from physical point of view. This typifies the thermal stability conditions of the materials under consideration and the onset of thermal runaway characteristics. To compute the criticality conditions in the system, we shall employ a very efficient solution method, known as Hermite-Padé approximants, which was first introduced by Padé [24] and Hermite [25].

We say that a function is an *approximant* for the series

$$S = \sum_{n=0}^{\infty} s_n\alpha^n \quad (19)$$

if it shares with S the same first few series coefficients at $|\alpha| < 1$. Thus, the simplest approximants are the partial sums of the series S. When the series converges rapidly, such *polynomial* approximants can provide good approximations of the sum.

Because of the continuation of analytical solution and dominating singularity behavior, the bifurcation study is performed using the partial sum of (19). The dominating behavior of the function $S(\alpha)$ represented by a series (19) may be written as

$$S(\alpha) \sim \begin{cases} B + A\left(1 - \dfrac{\alpha}{\alpha_c}\right)^\delta & \text{when } \delta \neq 0, 1, 2, \dots, \\ B + A\left(1 - \dfrac{\alpha}{\alpha_c}\right)^\delta \ln\left|1 - \dfrac{\alpha}{\alpha_c}\right| & \text{when } \delta = 0, 1, 2, \dots, \end{cases}$$

(20)

as $\alpha \to \alpha_c$, where A and B are some constants and α_c is the critical point with the critical exponent δ.

Assume that the $(d+1)$ tuple of polynomials, where d is a positive integer:

$$P_N^{[0]}, P_N^{[1]}, \dots\dots\dots\dots\dots, P_N^{[d]}$$

where, $\deg P_N^{[0]} + \deg P_N^{[1]} + \dots + \deg P_N^{[d]} + d = N$,

(21)

is a Hermite-Padé form of these series if

$$\sum_{i=0}^{d} P_N^{[i]}(\alpha) S_i(\alpha) = O\left(\alpha^N\right) \text{ as } |\alpha| < 1 \qquad (22)$$

Here $S_0(\alpha), S_1(\alpha), \dots\dots\dots\dots, S_d(\alpha)$ may be independent series or different form of a unique series. We need to find the polynomials $P_N^{[i]}$ that satisfy the equations (21) and (22). These polynomials are completely determined by their coefficients. So, the total number of unknowns in equation (22) is

$$\sum_{i=0}^{d} \deg P_N^{[i]} + d + 1 = N + 1 \qquad (23)$$

Expanding the left hand side of equation (22) in powers of α and equating the first N equations of the system equal to zero, we get a system of linear homogeneous equations. To calculate the coefficients of the Hermite-Padé polynomials it requires some sort of normalization, such as

$$P_N^{[i]}(0) = 1 \text{ for some integer } 0 \leq i \leq d \qquad (24)$$

It is important to emphasize that the only input required for the calculation of the Hermite-Padé polynomials are the first N coefficients of the series $S_0(\alpha), S_1(\alpha), \dots\dots\dots\dots, S_d(\alpha)$. The equation (23) simply ensures that the coefficient matrix associated with the system is square. One way to construct the Hermite-Padé polynomials is to solve the system of linear equations by any standard method such as Gaussian elimination or Gauss-Jordan elimination. In practice, one usually finds that the dominant singularities as well as the possibility of multiple solution branches for the nonlinear problem are located at zeroes of the leading polynomial coefficients $P_N^{[d]}(\alpha)$ of the equation (22). If the singularity is of algebraic type, then the exponent δ may be approximated by

$$\delta_N = d - 2 - \frac{P_N^{[d-1]}(\alpha_{c,N})}{D P_N^{[d]}(\alpha_{c,N})}. \qquad (25)$$

Drazin –Tourigney Approximants [26] is a particular kind of algebraic approximants and Khan [27] introduced High-order differential approximant (HODA) as a special type of differential approximants. More information about the above mentioned approximants can be found in the respective references.

5. Entropy Generation

The characteristics of the flow field inside a porous channel with isothermal walls in the presence of thermal radiation with viscous dissipation and MHD effect are irreversible. The exchange of energy and momentum within the fluid and at the boundaries causes inequilibrium conditions which leads to continuous entropy generation. Following Bejan [17] the volumetric entropy generation rate is given as

$$E_G = \frac{\kappa_\infty}{T_0^2}\left(\frac{d\bar{T}}{dy'}\right)^2 + \frac{\mu_{nf}}{T_0}\left(\frac{du'}{dy'}\right)^2 \qquad (26)$$

Where the first term on the right side of equation (26) is the irreversibility due to heat transfer and the second term is the irreversibility due to viscous dissipation. The entropy generation number can be expressed in dimensionless form as,

$$N_S = \frac{T_0^2 b^2 E_G}{\kappa_\infty (T_a - T_0)^2} = \left(\frac{d\theta}{dy}\right)^2 + \frac{Br}{\Omega(1-\phi)^{2.5}}\left(\frac{du}{dy}\right)^2$$
(27)

Where $\Omega = \frac{(T_a - T_0)}{T_0}$ is the temperature difference parameter and

$$N_1 = \left(\frac{d\theta}{dy}\right)^2, \quad N_2 = \frac{Br}{\Omega(1-\phi)^{2.5}}\left(\frac{du}{dy}\right)^2$$

In general, the entropy generation number N_s given in Eq. (27) provides a useful means of producing entropy generation profiles. However, it gives no indication as to the relative contributions of the fluid heat transfer and fluid friction effects. Thus, the parameter, Bejan number *Be* is commonly used in its place.

The Bejan number is given as $Be = \dfrac{N_1}{N_S}$

It is noteworthy that the Bejan number ranges from 0 to 1 and $Be = 0$ is the limit where the irreversibility is dominated by fluid friction effects. $Be = 1$ is the limit where the irreversibility due to heat transfer dominates the flow system because of finite temperature differences. The contributions of heat transfer and fluid friction to entropy generation are equal when $Be = \frac{1}{2}$. In the present work, second law analysis is investigated between a porous channel.

6. Results and Discussion

The influences of thermal radiation and temperature dependent variable thermal conductivity on the entropy generation of nanofluid flow through a porous channel under viscous dissipation effect in the presence of uniform magnetic field is studied in this paper. The numerical computation of series (18) subject to the boundary conditions (11) are carried out for various values of the physical parameters *Pr, R, Br, Gr, Re, Pe, Ha* and α to obtain the condition under which the dual (upper and lower branch) solutions may exist. The minimum entropy conditions provide the possibility of achieving the maximum available work.

In the present study, the nanoparticles volume fraction is specified in the range of $\phi = 0\% - 5\%$ to keep the physical properties of nanofluid stable, where a value of $\phi = 0$ indicates the pure base fluid. In addition, the thermal conductivity variation parameter is assigned in the range of $-0.1 \leq \alpha \leq 0.2$ due to the convergence of the series, Reynolds number (porosity parameter) $0 \leq Re \leq 8$ to control the intensity of porosity as physically stable and realizable, the radiation parameter $0 \leq R \leq 10$, the Brinkman number $1 \leq Br \leq 100$, the Hartmann number $0 \leq Ha \leq 4$ which is physically applicable as discussed in the available literature. The Grashof number and dimensionless pressure gradient are kept fixed at $Gr = 1, N = 1$.

Table 1 shows the comparison of our results with those of Makinde and Eegunjobi [22] with $Br = 0, Ha = 0, Gr = 0, Re = 1, N = 1$ for pure base fluid. The results in Table 1 imply that there is a good agreement of the values of velocity profile between the present study and Makinde and Eegunjobi [22] from the lower injected wall ($y = -1$) towards the centerline ($y = 0$) and then to upper suctioned wall ($y = 1$) of the channel.

Table 1. Comparison of numerical values for velocity with available literature when $Br=0, Ha=0, Gr=0, \phi=0, \text{Re}=1, N=1$

y	Present Study	Makinde and Eegunjobi [22]	Difference
-1.0	0	0	
-0.8	0.03894655	0.03879297	0.4%
-0.6	0.07258247	0.07114875	1.3%
-0.4	0.09765518	0.09639032	2%
-0.2	0.11658237	0.11376948	2.4%
0	0.12939390	0.12245933	5.3%
0.2	0.12553130	0.12154600	3.2%
0.4	0.11508405	0.11001953	4.4%
0.6	0.09134248	0.08676372	5%
0.8	0.05172775	0.05054498	2.3%
1.0	0	0	

6.1 Stability analysis

Table 2. Numerical calculations showing thermal conductivity criticality for different parameter values using High-order Differential Approximants at $Br=1, Gr=1, \phi=0, Ha=1, N=1$ for $d=3$.

R	Re	α_c	δ	Nu
1	0	-0.5356572	0.464278	0.18643029
2	0	-0.3773321	0.449667	0.55615580
5	0	-0.2164193	0.456544	1.13072342
1	3	0.0080012	0.456654	5.92068925
5	3	0.0072068	0.448767	6.01417978

Table 2 displays that the critical values of thermal conductivity variation parameter α_c increase with a positive increase in the values of radiation parameter R in absence of suction/injection parameter and the values of δ indicates that α_c is a branch point. On the

other hand, the presence of porosity parameter ($\text{Re}=3$) increases α_c positively.
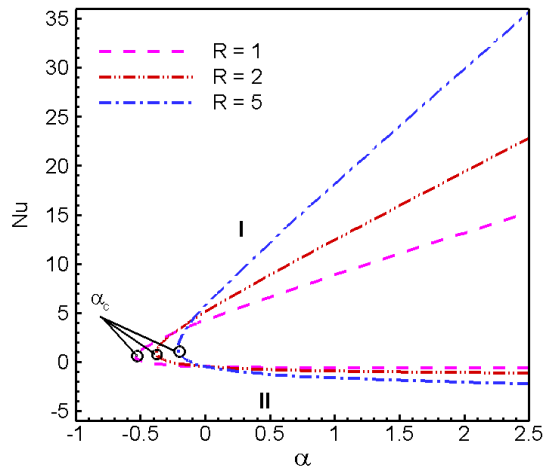
Fig.2. Approximate bifurcation diagrams of α in the $(\alpha, Nu(1))$ plane for different values of R obtained by Drazin-Tourigny method (1996) at $d=5, \phi=0, N=1, Ha=1, Gr=1, Br=1, \text{Re}=0$.

Therefore, it is significant to notice from the table that the progress of thermal runaway diminishes and develops thermal stability in the system when radiation effect enhances in porous wall. Moreover, the rate of heat transfer Nu enhances as R increases. Finally the values of α_c in Table 2 give an idea about the onset of thermal instability and its nature numerically. A segment of bifurcation diagram for different values of R in the (α, Nu) plane is noticed in Fig. 2 using Drazin-Tourigny Approximants at $\text{Re}=0$. It is interesting to notice that there are two solution branches (I and II) of Nusselt number when $\alpha > \alpha_c$, one solution when $\alpha = \alpha_c$, and no solution when $\alpha < \alpha_c$, where α_c is the critical value of α for which the solution exists. The stability analysis indicates that the lower solution branch (II) is stable and physically realizable. For different values of R, the upper solution

branch (I) is unstable and physically unacceptable shown in Fig. 2. Meanwhile, the positive variation of thermal conductivity parameter slowly decreases the rate of heat transfer and as *R* increases the bifurcating point increases and produces more instability to the upper solution branch (I). The numerical values in Table 2 are also consistent with the lower solution branch of *Nu* as *R* increases in Fig.2.

6.2 Effect of Reynolds number

Figures 3(a, b), 4(a, b) describes the effect of Reynolds number on flow characteristics with entropy generation within the channel. Figure 3(a) reveals that the velocity decreases with an increase in injection parameter as *Re* near the lower wall ($y = -1$) and the maximum velocity also develops towards the upper wall when *Re* increases due to suction. In absence of suction/injection parameter $(\text{Re} = 0)$, the velocity profile is parabolic and symmetrically distributed inside the channel; it however becomes skewed with increase in suction/injection parameter. Meanwhile, there occur backflow at the lower porous wall for large values of *Re*.   Fig.3(b) demonstrates a significant reduction in fluid temperature inside channel when *Re* increases. This is physically true since injection of fluid increases the fluid velocity around centerline thereby increases the heat transfer rate within the channel.

Generally, the value of N_2 i.e., the entropy generated by fluid friction is larger than that of N_1 i.e., the entropy produced by fluid heat transfer.
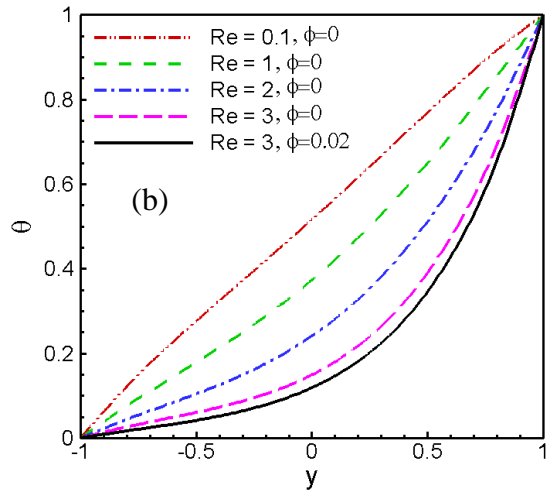

Fig.3. Effect of Reynolds number on (a) velocity profiles and (b) temperature distributions respectively
at
$$Br = 7.1, Gr = 1, \alpha = 0.1, \ N = 1, \Pr = 7.1, Ha = 1, R = 1.$$

As a result, N_S is contributed mainly by N_2 throughout the entire flow field. However, in the areas of the flow field characterized by a faster flow rate, the velocity gradient is reduced, and thus N_2 also reduces. In the present porous channel, N_S gradually reduces to zero at $y = 0$ as shown in Fig. 4(a).
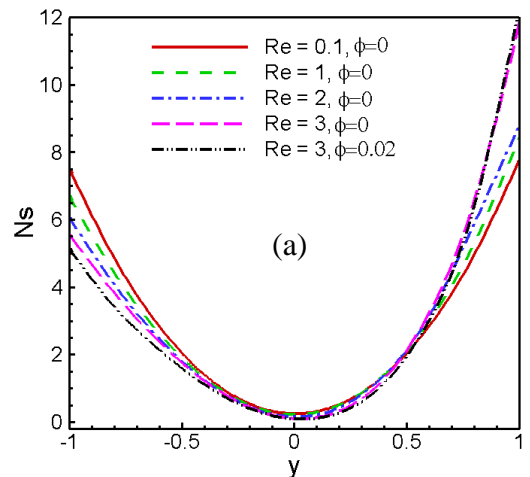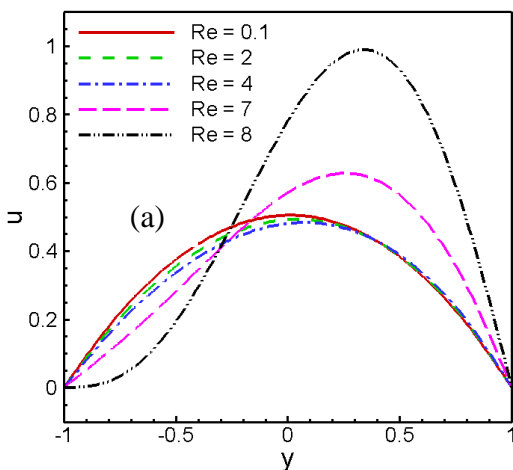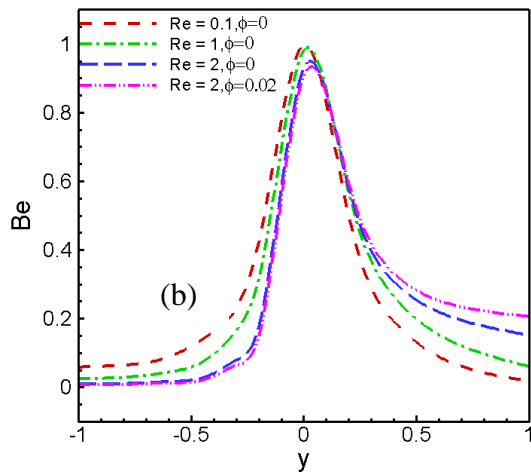
Fig.4. Effect of Reynolds number on (a) entropy generation rate and (b) Bejan profiles respectively at $Pr=7.1, Gr=1, Br=7.1, N=1, R=1, Ha=1, \alpha=0.1$.

In this particular region of the flow field, fluid friction effects play only a minor role, and thus N_S is contributed mainly by N_1. The figure reveals a minor decrease in N_s when Re increase near the cold porous wall, whereas N_S increases rapidly in base fluid and further in nanofluid in the region above the centerline to the upper hot porous wall. Since the dominant effect of heat transfer occurs at the upper hot wall. Figure 4(b) displays the distribution of the Bejan number (*Be*) versus the channel width for Reynolds number. It is noticed that *Be* has a value of zero at the lower cold wall and close to zero at the upper hot wall of the channel since, as discussed previously, the velocity gradient is increased at the walls due to suction/injection, and hence N_S is contributed mainly by N_2. In the central region of the flow field, *Be* increases to a maximum value of 1 due to the reduction in the velocity gradient and the corresponding increase in the contribution of N_1 to the overall entropy generation. It is to be seen that the heat transfer irreversibility dominates the flow process within the channel

centerline region, while the influence of fluid friction irreversibility can be observed at the two porous walls.

6.3 Effect of Thermal Conductivity variation parameter

The influences of thermal conductivity variation parameter on temperature distribution, entropy generation rate N_s and distribution of Bejan number *Be* are depicted in Figs. 5(a, b, c). A decrease in the fluid temperature around the central region of the channel is observed in Fig. 5(a) due to the positive escalating values of α. The temperature profile is further decreased in nanofluid than base fluid as α increases. The increases of thermal conductivity variation parameter produce more heat transfer within the channel centerline region and reduce dimensionless temperature distribution. Furthermore, due to the higher thermal conductivity coefficient of the nanofluid, the heat is more keenly transferred. Fig. 5(b) indicates the effect of thermal conductivity variation parameter on entropy generation number inside the channel. From this figure, it is observed that near the cold porous wall, N_s decreases slightly with the increase of α while it increases with the increase of α toward the hot porous wall. The influence of thermal conductivity variation parameter on Bejan profile is seen in Fig. 5(c).
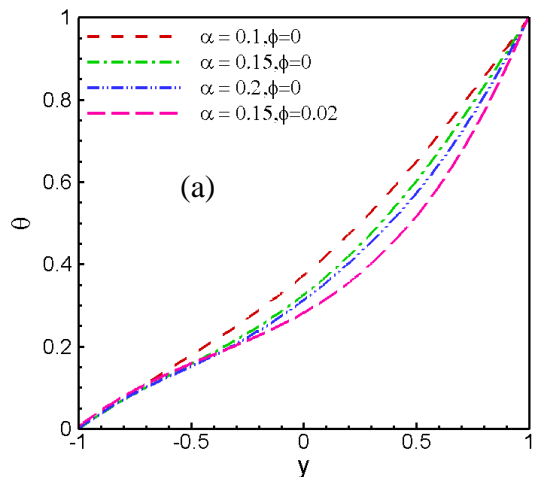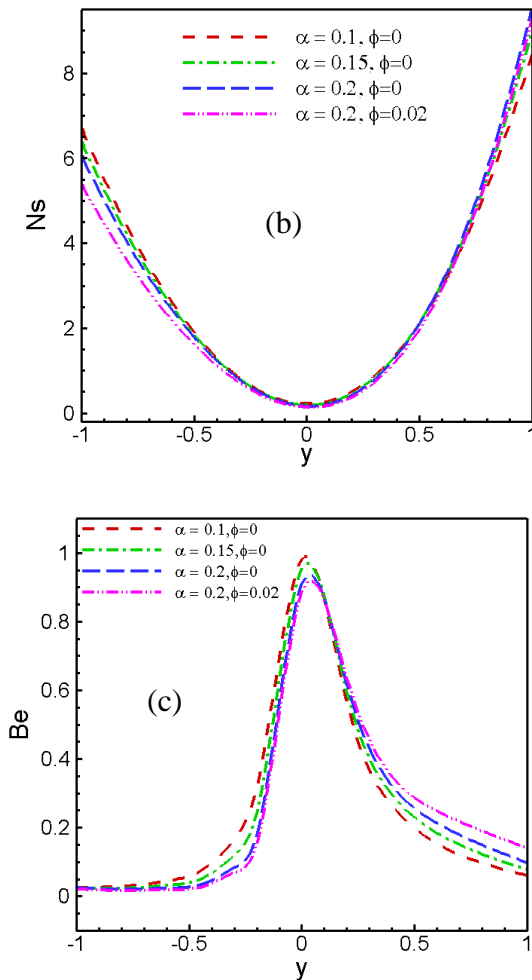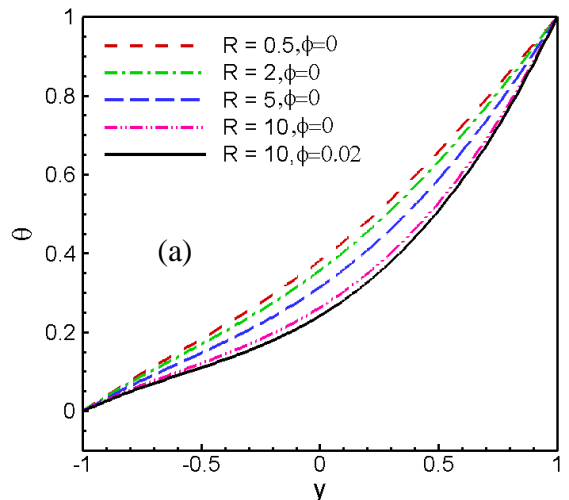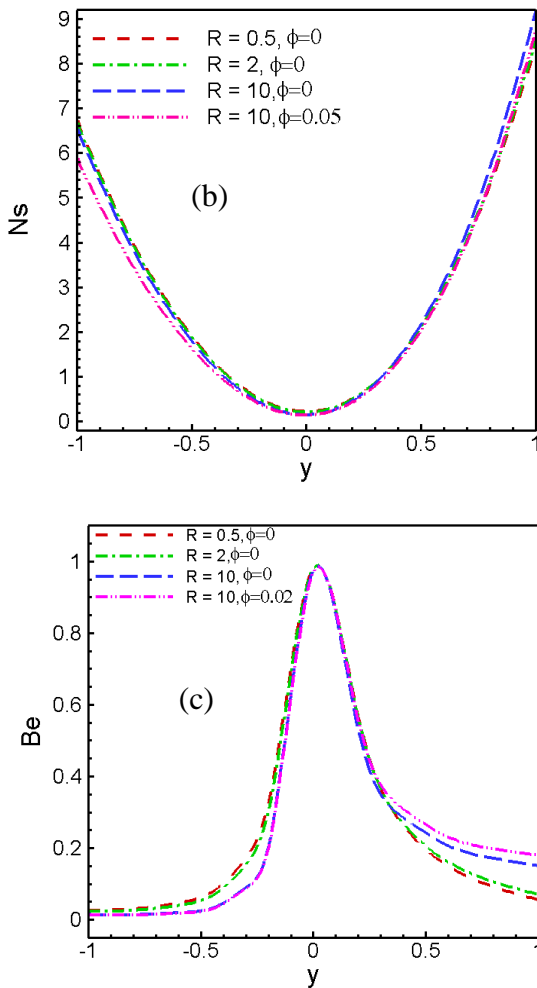
Fig.5. Effect of thermal conductivity variation parameter on (a) temperature profile, (b) entropy generation rate and (c) Bejan profiles respectively at $Pr=7.1, Gr=1, Br=7.1, N=1, Re=1, Ha=1, R=1$.

It can be noted from this figure that fluid friction irreversibility dominates entropy generation near the porous walls while heat transfer irreversibility is the dominant contributor near the channel centerline. It is observed that as α increases, the dominance of heat transfer irreversibility near the hot wall increases especially for nanofluid while the dominance of fluid friction irreversibility near the cold porous wall is insensitive to change in α.

6.4 Effect of Radiation parameter

Figures 6(a, b, c) represent the flow characteristics with entropy generation due to the effect of Radiation parameter. The effect of Radiation parameter R on fluid temperature in Fig. 6(a) shows that temperature near the channel centre line reduces uniformly by the positive increase of R due to radiative heat loss. Also nanofluid enhances the rate of heat transfer which leads to more reduction in temperature as reflect in Fig. 6(a). Entropy generation due to the effect of radiation parameter R is shown in Fig. 6(b). The figure reveals a small decrease in N_s when R increase near the cold porous wall, whereas N_s increases significantly toward the hot porous wall because of the sole contribution of heat transfer effect. Figure 6(c) displays the distribution of Bejan number for different values of Radiation parameter R. The figure instructed that as R increases, there is enhanced dominance of heat transfer irreversibility near the hot porous wall where nanofluid exhibits the maximum. There is an absolute dominance of heat transfer irreversibility $(Be=1)$ for varying values of R near the centerline of the channel while there absolute dominance of fluid friction irreversibility $(Be=0)$ near the cold porous wall.
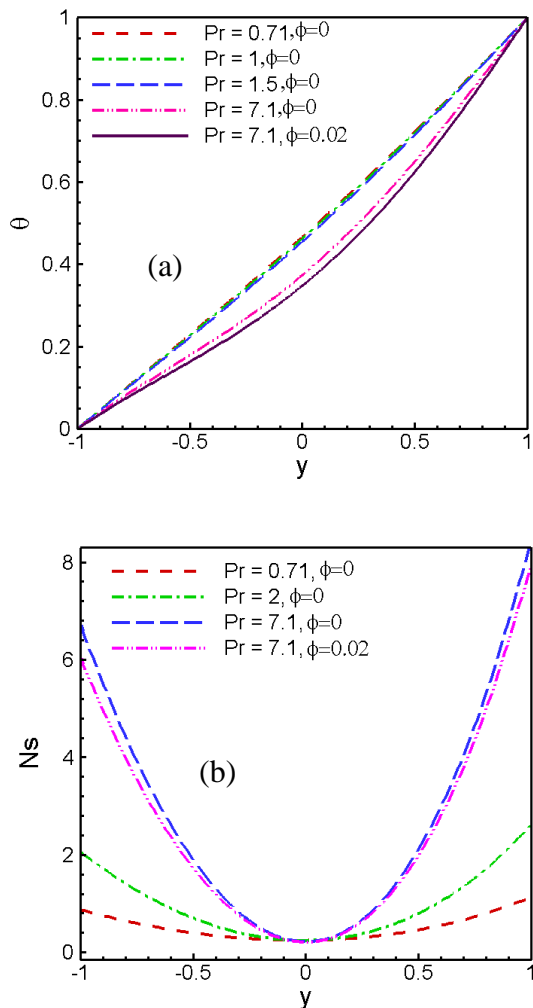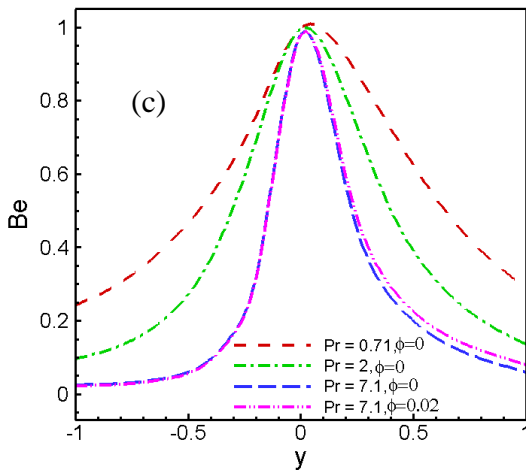
Fig.6. Effect of Radiation parameter on (a) temperature profile, (b) entropy generation rate and (c) Bejan profiles respectively at Pr=7.1, Gr=1, Br=7.1, N=1, Re=1, Ha=1, α=0.1.

6.5 Effect of Prandtl number

The effects of Prandtl number on temperature distribution, entropy generation rate N_S and distribution of Bejan number *Be* are depicted in Figs. 7(a, b, c). The temperature of fluid inside the channel decreases rapidly for base water and further in Cu-water nanofluid than air or other gases due to higher thermal conductivity coefficient as observed in Fig. 7(a). The effect of Prandtl number *Pr* on entropy generation rate is noticed in Fig. 7(b). The figure reveals an increase in N_S as *Pr* increases near the porous walls. This is

due to the increase in temperature gradient as *Pr* increases which is also further in nanofluid. In Fig. 7(c) Bejan number is represented for various values of Prandtl number *Pr*. It is noticed from the figure that the dominance effect of both fluid friction and heat transfer irreversibility near the two walls almost similar. On the other hand, the dominance effect of fluid friction irreversibility is absolute near the porous walls and the dominance of heat transfer irreversibility decreases as *Pr* increases for base water and Cu-water nanofluid. The conjecture of Figs 7 (b, c) has a good agreement with those results of Abiodun et al. [21].

Fig.7. Effect of Prandtl number on (a) temperature profile, (b) entropy generation rate and (c) Bejan profiles respectively at $R=1, Gr=1, Br=7.1, N=1, \mathrm{Re}=1, Ha=1, \alpha=0.1$.

6.6 Effect of Hartmann number

Figure 8 represents that in absence of magnetic field velocity achieves its maximum value, while increasing values of *Ha* produces reduction of the velocity near the channel centerline region. The variation of *Ha* leads to the variation of the Lorentz force due to magnetic field and the Lorentz force produces more resistance to the fluid velocity.
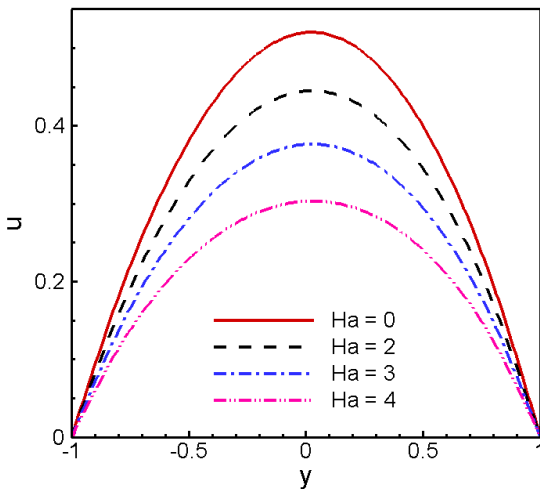
Fig.8. Effect of Hartmann number on velocity profile at $Br=7.1, Gr=1, \alpha=0.1,$ $\mathrm{Re}=1, R=1, \mathrm{Pr}=7.1, \phi=0$

6.7 Effect of nanoparticles volume fraction

The influence of nanoparticles volume fraction ϕ on velocity is depicted in Fig.9 at $\mathrm{Re}=1$. In Fig.9, a uniform reduction in fluid velocity is observed as ϕ increases. The equivalent thermal expansion coefficient of the nanofluid is less than that of base water. As a result, the buoyancy force acting on the nanofluid is also less than that acting on the pure water, and hence the dimensionless velocity is reduced. In addition, since the density and viscosity of the nanofluid are greater than those of base water, the velocity distribution within the channel is more uniform.
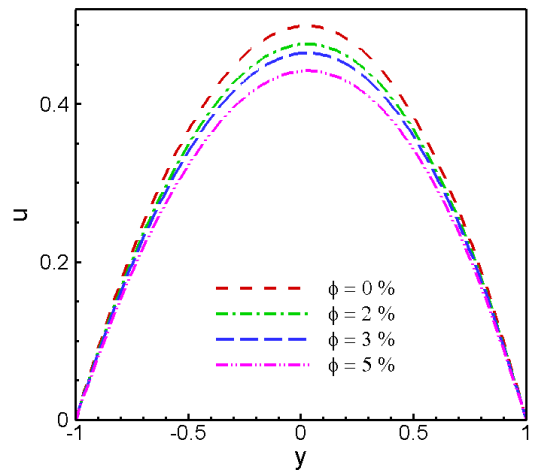

Fig.9. Effect of nanoparticles volume fraction on velocity profiles at $Br=7.1, Gr=1, \alpha=0.1,$ $\mathrm{Re}=1, R=1, \mathrm{Pr}=7.1, Ha=1$.

6.8 Effect of Brinkman number

The dimensionless velocity distribution of the flow field has a direct effect on the dimensionless temperature distribution as the effects of viscous dissipation are taken into consideration in the present problem. It is noticed from Fig.10 that the fluid temperature increases with increasing parametric values of viscous heating parameter *Br* but a minor reduction is

seen in presence of nanoparticles. The velocity gradient of the pure working fluid is greater than that of the nanofluid due to the lower viscosity which results in more viscous dissipation effect. Furthermore, due to the higher thermal conductivity coefficient of the nanofluid, the heat is more intensely transferred. Hence, the dimensionless temperature of the nanofluid is less than that of the base fluid in Fig. 10.
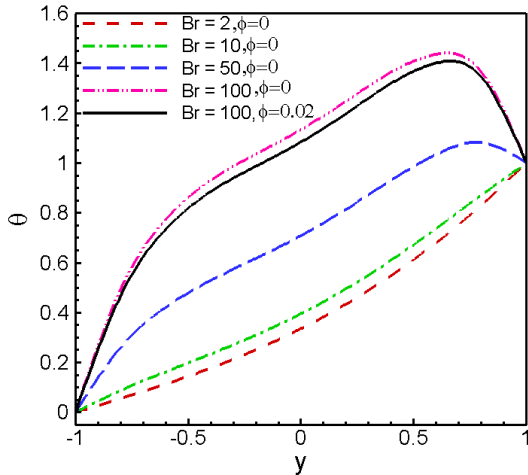
Fig. 10. Effect of Brinkman number on temperature profile
at $R=1, Gr=1, N=1, \Pr=7.1 \ Re=1, Ha=1, \alpha=0.1.$

7. Conclusion

In this paper the radiative heat transfer on the entropy generation of MHD steady variable thermal conductivity flow and heat transfer with viscous dissipation of Cu-water nanofluid through a porous channel is investigated. Applying Hermite- Padé approximation method, the dominating singularity behaviour of the problem as well as the existence of the dual solutions of the rate of heat transfer is examined. It is observed that suction/injection of fluid exerts a significant influence on the velocity and temperature distributions, which transitively affects the entropy generation within the channel. The major conclusions of the present problem are

➢ For $\alpha > \alpha_c,$ the solution of rate of local heat transfer has two branches,

namely, an upper branch and a lower branch. It is found that at the lower solution branch which is physically acceptable, the value of Nusselt number decreases with the increase of radiation parameter.

➢ At the lower porous wall, there occurs backflow as the porosity parameter *Re* increases. An increase in the thermal conductivity variation parameter and Radiation parameter reduces temperature distribution due to faster heat loss. Increasing Hartmann number and nanoparticles solid volume fraction cause the reduction of fluid velocity near the centerline uniformly because of the acting of Lorentz force and reduction of buoyancy force.

➢ For regions of the flow field at a greater velocity gradient, i.e., adjacent to the porous walls, the total entropy generation rate is dominated by the effects of fluid friction. Moreover, in the regions of the flow field at a greater and more uniform velocity distribution, i.e., the central region of the channel, the total entropy generation rate is dominated completely by the effects of fluid heat transfer.

8. Nomenclature

B_0	magnetic induction
b	dimensional channel length
Br	Brinkman number
C_p	specific heat
g	gravitational acceleration
Gr	Grashof number
Ha	Hartmann number
N	dimensionless pressure gradient
Nu	local Nusselt number
p'	dimensional pressure
P	dimensionless pressure
R	Radiation parameter
T_0	ambient temperature

$\bar{T}$	dimensional temperature
T_a	hot temperature
u'	velocity component along the x' axes
u	dimensionless velocity
v'	velocitycomponent along the y' axes

9. Acknowledgement

10. References

[1] Wernert, V., Schaf, O., Ghobarkar, H. and Denoyel, R., Adsorption Properties of Zeolites for Artificial Kidney Applications, Microporous and Mesoporous Materials, Vol. 83, No. 1, pp. 101-113, 2005.

[2] Jafari, A., Zamankhan, P., Mousavi, S. and Kolari, P., Numerical Investigation of Blood Flow. Part ii: in Capillaries, Communications in Nonlinear Science and Numerical Simulation, Vol. 14, No. 4, pp. 1396-1402, 2009.

[3] Goerke, A.R., Leung, J. and Wickramasinghe, S.R., Mass and Momentum Transfer in Blood Oxygenators, Chemical Engineering Science, Vol. 57, No.11, pp. 2035-2046, 2002.

[4] Berman, A.S., Laminar Flow in Channels with Porous Walls, Journal of Applied Physics, Vol. 24, No. 9, pp. 1232-1235, 1953.

[5] Cogley, A.C.L., Vincenti, W.G. and Gilles, E.S., Differential Approximation for Radiative Heat Transfer in a Nonlinear Equations-grey Gas Near Equilibrium, Am. Inst. Aeronaut. Astronaut. J., Vol. 6, pp. 551-553, 1968.

[6] Chawla, T.C. and Chan, S.H., Combined Radiation and Convection in Thermally Developing Poiseuille Flow with Scattering, J. Heat Transfer, Vol. 102, pp. 297-302, 1980.

[7] Kay, W.M., Convective Heat and Mass Transfer, Mc-Graw Hill, New York, 1966.

[8] Pinarbasi, A., Ozalp, C. and Duman, S., Influence of Variable Thermal Conductivity and Viscosity for Nonisothermal Fluid Flow, Physics of Fluids, Vol. 17, No. 3, 2011.

[9] Moreau, R., Magnetohydrodynamics, Kluwer Academic Publishers, Dordrecht, 1990.

[10] Makinde, O.D., Magneto-hydrodynamic Stability of Plane-Poiseuille Flow using Multi-deck Asymptotic Technique, Math. Comput. Model, Vol. 37, No. 3-4, pp. 251-259, 2003.

[11] Patra, R., Das, S. and Jana, R.N., Radiation Effect on MHD Fully Developed Mixed Convection in a Vertical Channel with Asymmetric Heating, J. Applied Fluid Mechanics, Vol. 7, No. 3, pp. 503-512, 2014.

[12] Kwak, K. and Kim, C., Viscosity and Thermal Conductivity of Cupper Nanofluid Dispersed in Ethylene Glycol, Korea-Aust. Rheol. J., Vol. 17, pp. 35-40, 2005.

[13] Khanafer, K., Vafai, K. and Lightstone, M., Buoyancy-driven Heat Transfer Enhancement in a Two-dimensional Enclosure Utilizing Nanofluids, Int. J. Heat Mass Transfer, Vol. 46, pp. 3639-3653, 2003.

[14] Choi, S.U.S., Enhancing Thermal Conductivity of Fluids with Nanoparticles, in: Proceedings of the ASME International Mechanical Engineering Congress and Exposition, ASME, San Francisco, USA, Vol. 66, pp. 99-105, 1995.

[15] Das, S.K., Choi, S.U.S. and Patel, H.E., Heat Transfer in Nanofluids-a Review, Heat Transfer Eng, Vol. 27, No.10, pp. 3-19, 2006.

[16] Sheikholeslami, M., Ganji, D.D., Rokni, H.B., Nanofluid Flow in a Semi-porous Channel in the Presence of Uniform Magnetic Field, Int. J. of Engineering, Vol. 26, No.6, pp. 653-662, 2013.

[17] Bejan, A., Entropy-generation Minimization, CRC Press, New York, 1996.

[18] Bejan, A., A Study of Entropy Generation in Fundamental Convective Heat Transfer, J. Heat Transfer, Vol. 101, pp. 718-725, 1979.

[19] Makinde, O.D., Hermite-Padé Approach to Thermal Radiation Effect on Inherent Irreversibility in a Variable Viscosity Channel Flow, Comp. and Math. with Applications, Vol. 58, pp. 2330-2338, 2009.

[20] Chen, C.K., Chen, B.S. and Liu, C.C., Heat Transfer and Entropy Generation in Fully-developed Mixed Convection Nanofluid Flow in Vertical Channel, Int. J. Heat Mass Transfer, Vol.79, pp. 750-758, 2014.

[21] Abiodun, O.A., Basant, K.J. and Andrew, O., Entropy Generation under the Effect of Suction/injection, Applied Mathematical Modelling, Vol. 35, pp. 4630-4646, 2011.

[22] Makinde, O.D. and Eegunjobi, A.S., Effects of Convective Heating on Entropy Generation Rate in a Channel with Permeable Walls, Entropy, Vol. 15, pp. 220-233, 2013.

[23] Sheikholeslami, M., Soleimani, S., Gorji-Bandpy, M., Ganji, D. and Seyyedi, S., Natural Convection of Nanofluids in an Enclosure between a Circular and a Sinusoidal Cylinder in the Presence of Magnetic Field, Int. Com. in Heat and Mass transfer, Vol. 39, No. 9, pp. 1435-1443, 2012.

[24] Padé, H., Sur la Représentation Approchée d'une Fonction Pour Des Fractions Rationnelles, Ann. Sci. École Norm. Sup. Suppl., Vol. 9, pp. 1-93, 1892.

[25] Hermite, C., Sur la Généralisation Des Fractions Continues Algébriques, Annali di Mathematica Pura e Applicata, Vol. 21, No.2, pp. 289-308, 1893.

[26] Drazin, P.G. and Tourigny, Y., Numerically Study of Bifurcation by Analytic Continuation of a Function Defined by a Power Series, SIAM Journal of Applied Mathematics, Vol. 56, PP.1-18, 1996.

[27] Khan, M.A.H., High-Order Differential Approximants, Journal of Computational and Applied Mathematics, Vol. 149, pp. 457-468, 2002.